INCIPIENT BUFFET OVER LAMINAR-FLOW AIRFOIL - A DNS STUDY AT MODERATE REYNOLDS NUMBERS

M. Zauner and N.D. Sandham

University of Southampton
m.zauner@soton.ac.uk

Abstract

In order to study transonic buffet over aircraft wings, the linear stability of the flowfield is analysed based on direct numerical simulations at moderate Reynolds numbers. A significant change of the boundary layer stability depending on the aerodynamic load of the airfoil is suggested by local linear stability theory. Besides Kelvin Helmholtz instabilities, a global mode, showing the coupled dynamics of the separation bubbles, can be identified in agreement with literature. Both modes are present in a dynamic mode decomposition (DMD) of the unsteady direct numerical solution. Furthermore, DMD picks up the buffet-mode at a Strouhal number of $St = 0.12$ that agrees with experiments. Two additional modes with similar structure are observed at $St = 0.45$ and $St = 0.6$, suggesting that the observed buffet might involve triadic mode interactions, rather than being a single global mode.

1 Introduction

Transonic buffet is characterised by a structural response to an aerodynamic excitation produced by separated flows interacting with shock waves. It is of great interest to be able to define buffet-boundaries as precisely as possible in order to fully exploit and potentially extend the safe flight envelope. However, despite large experimental efforts, the self-sustaining mechanism is still not fully understood [1] [2]. Significant oscillations of aerodynamic loads can be observed on rigid wings as well, so it is generally assumed that the structural response of the wing is triggered by resonance effects after the disturbance amplitude reaches a sufficient magnitude. In the current work, direct numerical simulations (DNS) are performed over wing-sections at moderate Reynolds numbers up to $Re = 500{,}000$ (based on the chord length c) and a Mach number of $M = 0.7$ considering Dassault Aviation's V2C profile [3]. In the course of the TFAST project experimental as well as numerical analysis has been carried out on that profile under buffet conditions [4][5][6]. [7] characterises transonic buffet as a global mode, caused by a coupled modulation of a steady shockwave and the separated shear layer. There is great interest on global stability analysis of buffeting airfoils (i.e. [8][9][10]), but very little work has been done to date using DNS data. Based on recent results, we want to extend the investigations for the V2C profile, exploring the lower buffet boundary at 4° incidence and reduced Reynolds numbers.

2 Methodology

All direct numerical simulations were carried out using the high-order fully-parallelised multi-block finite difference in-house code SBLI with details in [11][12]. The dimensionless Navier-Stokes Equations (NSE) are solved by a fourth order finite difference scheme in space and a low-storage third-order Runge-Kutta scheme in time. The temperature dependency of the dynamic viscosity is modelled by Sutherland's law. Zonal characteristic boundary conditions are applied at the outflow boundaries, while integral characteristic boundary conditions at the remaining domain boundaries avoid reflections of shock- and pressure-waves. In the farfield, an implicit sixth-order filter increases the numerical stability of the simulation near strong pressure waves and suppresses spurious disturbances. A total variation diminishing (TVD) scheme is used to capture shock waves, but is disabled in boundary layers and near the leading edge. The computational domain is divided into three blocks consisting of one C-block around the airfoil geometry and two H-blocks enclosing the wake-region and outflow. In order to include the blunt trailing edge of the original profile, while maintaining continuous metric terms up to the second order of derivatives, an open-source grid generator was developed and released on GitHub [13]. The reference grid consists of more than one billion points, considering a spanwise domain width of $5\%c$. The adequacy of the grid resolution is confirmed by a grid-refinement study, based on a spectral error-indicator analysis identifying critical regions in terms of grid-to-grid point oscillations [14].

In order to analyse the linear stability, the flowfield is decomposed into a steady baseflow with superimposed disturbances. The baseflow is obtained from time- and span-averaged DNS solutions, whereas the disturbances are modelled by a normal-mode ansatz. For local linear stability theory, the Orr-Sommerfeld equations (involving parallel-flow assumptions on the linearised NSE) are solved for a 2D flowfield using the in-house code NoSTRANA [11]. Applying a temporal approach, the solution of an eigenvalue problem provides the temporal growth rate corresponding to an angular frequency for a given set of streamwise and

spanwise wave numbers. More details on this methodology and flow assumptions are provided by [15]. For the global stability analysis, the 2D linearised NSE are solved directly, applying a normal mode ansatz with prescribed spanwise wavenumbers. The large-scale eigenvalue problem is solved using the open-source software SLEPc [16] in combination with SBLI. More details on this approach are provided by [12]. In order to compare the calculated stability results with the unsteady direct numerical solution of the flowfield, the streaming dynamic mode decomposition method is applied [17] [18].

3 Unsteady flow structures

The reference simulation at $Re = 500{,}000$ shows a distinct supersonic region over the upper airfoil surface [19]. Two dimensional (2D) simulations already show the formation of strong Kelvin-Helmholtz vortex structures in the airfoil aft section, initialised by upstream moving pressure waves (also known as Kutta waves) that are caused by the von Karman vortex street, which first appear with Strouhal numbers of $St = fc/U_\infty \approx 36.5$. This suggests a complex cascade mechanism, also involving shock-wave/boundary-layer interaction and the Doppler effect, that allows flow structures of high frequencies to interact with flow phenomena at significantly lower frequencies. After extruding the 2D solution, a self-sustaining laminar/turbulent boundary-layer transition mechanism sets in on both sides without further artificial excitation of the flowfield. A transition mechanism similar to [20] can be observed, where vortex-stretching of near-wall streaks that are lifted up by strong 2D vortices promotes a rapid breakdown to turbulence (inset of figure 1). A 2D-like silhouette of the strong vortices can be still observed in the fully turbulent section. Furthermore, those turbulent structures interact with each other as well as the potential flow. In the aft section of the airfoil, strong acoustic radiation can be observed from multiple sources. Black contours in figure 1 indicate strong pressure gradients. Approaching the supersonic region, upstream-propagating acoustic pressure waves seem to accumulate and form stronger pressure waves (PW). Eventually, those pressure waves turn into shock waves (SW) and propagate upstream. Acoustic waves, circumventing the supersonic region, introduce additional disturbances into the supersonic region from above. A complex interaction between shock waves, introduced pressure waves and reflections at the boundary layer is observed. One can also observe Mack-like wave patterns (MW) on both sides that are caused by acoustic waves travelling upstream within the separated boundary layer (highlighted magenta in figure 1). Eventually, a distinct low-frequency oscillation in the lift-coefficient (up to 12% deviation from the mean value) is observed at a Strouhal number of $St = 0.12$, which is of the order of typical buffet frequencies [1]. Figure 2 shows the lift coefficient C_L as a function of time. The low-frequency behaviour can also be clearly observed in pressure signals as a function of time at various locations along the surface, including at the leading- and trailing-edges [19]. Low-frequency cycles can also be observed in the freestream on the pressure side of the airfoil [15]. There is no obvious correlation to pressure- or shock-waves detected, as they are generated at significantly higher frequencies. A more detailed discussion on the unsteady flow phenomena is given in [3] and [19].

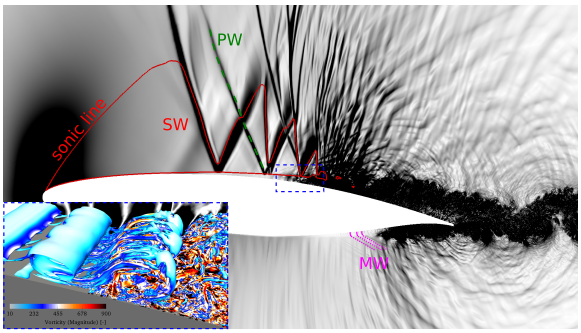

Figure 1: Magnitude of pressure gradient ($|\frac{\partial p}{\partial x}| + |\frac{\partial p}{\partial y}|$) (white $= 0$, black $= 1$), where the red curve denotes the sonic line. Sketched lines mark described flow phenomena. The insert shows Q-criteria surfaces coloured by vorticity of the upper transition region outlined by the blue dashed rectangle.

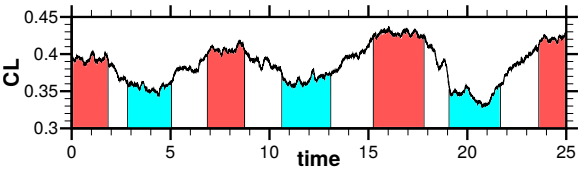

Figure 2: Lift coefficient C_L as a function of time. High-lift phases (HLP) and low-lift phases (LLP) are highlighted in red and blue, respectively.

4 Local and global linear stability

From the analysis of unsteady behaviour, [3] reported Kelvin-Helmholtz instabilities at Strouhal numbers of $St \approx 20$. Similar flow structures ($St \approx 25$) in a simulation of a high-pressure turbine vane could also be associated with linear instabilities by [15]. A similar method is applied here to the time- and span-averaged flowfield of the suction side of a direct numerical simulation, denoted as case $C0$[3] with a total run time of 25 time units (one time unit is defined as the chord length over the freestream velocity). As a consequence of the observed incipient buffet phenomenon, the flowfield and in particular the boundary- and shear-layers change significantly. The top and middle contour-plots of figure 3 show the z-vorticity

component (ω_z) of phase-averaged baseflows considering only high-lift phases (HLP) or low-lift phases (LLP), respectively. The time-segments that are considered for high- and low-lift phases are highlighted red and blue respectively in figure 2. Due to the limited number of simulated low-frequency cycles, there are still traces of instantaneous flow features (especially in the freestream) that are not completely averaged out. During low-lift phases, the separation bubble moves upstream and the flow separation becomes more pronounced. Iso-curves in the bottom plot of figure 3 show a direct comparison of the shear layers for HLP (red) and LLP (blue). For HLP, flow follows the contour longer, whereas the shear at the lower corner of the blunt trailing edge is significantly reduced. The shear-layer along the suction side surface does not change that significantly. Using a baseflow that is av-

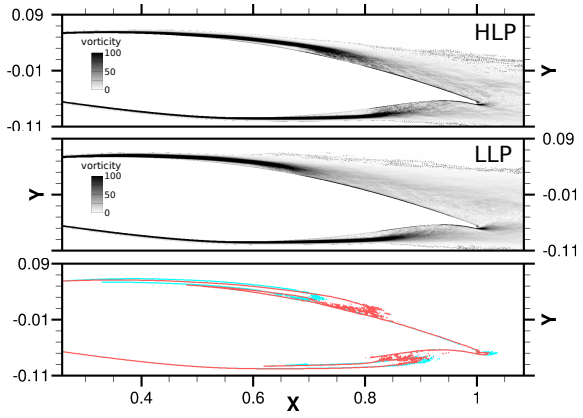

Figure 3: Phase-averaged vorticity fields for high-lift phase (top) and low-lift phase (middle). Iso-curves for $\omega_z = 50$ of high-lift phase and low-lift phase in red and blue, respectively.

eraged over the total run time of the simulation, comprising those high- and low-lift phases, removes potentially important information. Therefore the phase averaged base flows shown in figure 3 are also analysed with respect to linear instabilities. This is justified on the ground that there still exists a wide frequency separation between the buffet mode and the KH modes. Figure 4 shows the temporal growth rate (ω_i) as a function of surface distance s for an angular wave number of $\omega_r = 125$, considering only 2D modes (spanwise wavenumber $\beta = 0$). The wavy pattern is likely to be due to upstream-moving pressure waves interacting with the boundary layer and insufficient time averaging. We can clearly see that the total time average (black curve) underestimates linear instabilities in comparison to high- (red curve) and low-lift (blue curve) phases. Compared to LLP, the boundary layer at HLP shows higher temporal growthrates peaking closer to the trailing edge. Instantaneous snapshots confirm that KH roll-ups form further upstream at LLP.

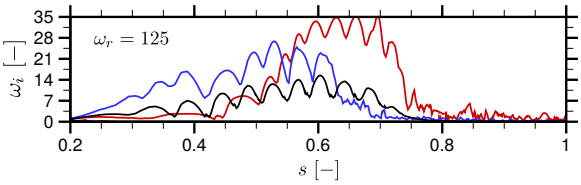

Figure 4: Temporal growth rate ω_i as a function of the chord position for an angular frequency of $\omega_r = 2\pi \cdot St = 125$. The line colour corresponds to time- and span-averaged baseflows over high-lift phases (red), low-lift phases (blue) and the full run time (black).

Considering the flow around a NACA 0012 airfoil at $Re = 200{,}000$ and $M = 0.4$, [21] reports a region in the spectrum that is dominated by distinct equally-spaced frequencies (tonal noise) around a maximum peak at $St \approx 7$ that corresponds to a stable global mode. An impulse response analysis by [22] showed the vivid interaction between suction and pressure side at that frequency and suggested a feedback mechanism due to pressure waves that are scattered at the trailing edge and form upstream moving acoustic waves. A similar stable mode can be observed in preliminary global stability results of the current test case at $St = 5.89$ suggesting a growth rate of $\omega_i = -0.019$ (negative growth rates denote damping). The divergence field of that global mode in figure 5(a) shows regions of high growth rates in the separation regions on both sides. This global mode also involves upstream-travelling acoustic waves originating at the trailing edge. While those waves can travel along the pressure side without any restrictions, they are slowed down on the suction side approaching the supersonic region. Near the shock wave that bounds the supersonic region in the downstream direction, those waves are compressed as the phase speed decreases to zero. The pressure waves circumventing the supersonic region slide along the sonic line and introduce disturbances that are reflected at the airfoil surface. This mode seems to describe a dynamic coupling between separation regions and the trailing edge, via upstream moving pressure waves. The z-vorticity of this eigenmode is shown in figure 5(b).

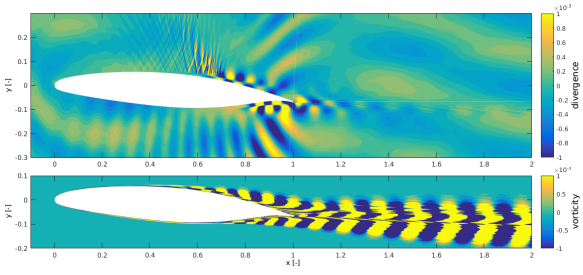

Figure 5: Divergence field (top) and vorticity field (bottom) of a global mode at $St = 5.89$.

5 Dynamic mode decomposition

A dynamic mode decomposition (DMD) is performed considering two sets of 2D snapshots over 25 time units in the xy-plane as well as an xz-plane (located within the shear layers). Figure 6 shows the normalised amplitude as a function of St for DMD modes corresponding to one set of 1249 snapshots with a step size of 0.02 time units (top plot) and another set of 124 snapshots with a step size of 0.1 time units (bottom plot). The eigenfunctions of the modes marked red are shown in figure 7, plotting contours of density (left column) and streamwise velocity component (right column). The top row shows a mode at $St = 19.3$, picking up the KH roll-ups, which are associated with linear instabilities. The shape of the eigenmode is reminiscent of structures that are observed in movies and snapshots like figure 1. Figure 6 shows several modes at frequencies between $15 < St < 25$ with similar or even higher amplitudes with similar shapes of eigenmodes. Considering the results of the linear stability analysis, the frequency of the KH instabilities is expected to vary significantly due to the dynamics of the flowfield.

The density-field corresponding to an eigenmode at a Strouhal number of $St = 6.3884$ is shown in the second row of figure 7. The results agree with the global stability analysis of the previous section. There are big turbulent vortices observed downstream

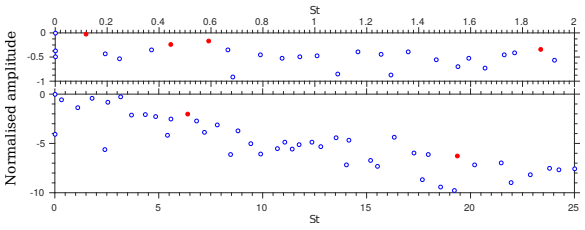

Figure 6: Normalised amplitude of DMD modes as a function of their Strouhal number.

of the laminar/turbulent transition region with Strouhal numbers around $St = 1.8$. These modes can also be found in the DMD spectrum. The density field in the third row of figure 7 shows strong oscillations in the aft section of the airfoil and in the wake. In addition, upstream-moving pressure waves, originating at the trailing edge can be observed. A phase-shift of the oscillations within the upper-side shear layer and the freestream can be seen in the velocity field of that mode.

Besides the low-frequency peak at $St = 0.12$ (last row of figure 7) corresponding to the buffet phenomenon, distinct low-frequency modes at $St = 0.6$ and $St = 0.45$ are shown in the second last row of figure 7. At these frequencies, the formation of shock waves moving upstream into the supersonic region is observed [3]. The Fourier spectrum shows distinct equidistant peaks in that frequency range [19]. Both eigenmodes look similar, but have a clear phase shift. Those modes seem to be strongly coupled with the shock dynamics and the flapping of the wake. Whereas the mode at $St \approx 0.6$ shows the highest amplitudes on the lower side of u in the near wake, the mode at lower frequencies suggests that peak on the airfoil aft section of the pressure side. This might be an indicator that the mode at $St \approx 0.6$ is dominant on the suction side and disturbances move around the trailing edge upstream along the pressure side (see density plot in figure 7), whereas the mode at $St \approx 0.45$ is playing a more active role on the pressure side. The frequency of a mode at $St = 0.12$ (in the last row of figure 7) agrees with typical transonic buffet frequencies in literature and can also be extracted from the lift coefficient over time. The eigenmode involves basically the same regions as the two modes at $St \approx 0.45$ and $St \approx 0.6$. In the velocity field, the suction and pressure sides are clearly separated by a phase shift, indicating an opposed streamwise oscillation of the shear layers. Density fluctuations of the modes with $St < 1$ are not only observed in the streamwise direction, but also in the wall-normal direction.

6 Discussion

DNS data has been analysed in terms of local and global linear stability in order to investigate the transonic buffet mechanism of a narrow wing section at 4° angle of attack and Mach and Reynolds numbers of $M = 0.7$ and $Re = 500{,}000$, respectively. Local linear stability theory associates KH roll-ups with convective linear instabilities, agreeing with literature for a high-pressure turbine vane at similar freestream conditions. The shear layer on the suction side shows significantly different characteristics during high- and low-lift phases. The analysis of the time- and span-averaged flowfield underestimates the growth rates of those instabilities compared to phase-averaged baseflows, corresponding to HLP and LLP. At HLP, the unstable region in the boundary layer is further upstream, with higher growth rates at higher frequencies, compared to LLP. Preliminary global stability analysis captures a tonal mode at $St = 5.89$ that has been previously reported in literature with respect to coupled dynamics of separation bubbles [22]. As the global stability analysis continues, we expect to find more global modes. Dynamic mode decomposition is able to capture the KH instabilities as well as the global mode at $St = 5.89$. Furthermore, the DMD shows eigenmodes at $St = 1.87$ that are associated with large turbulent vortices in the suction-side aft section of the airfoil. Those roll-ups seem to be coupled with the shock region and large-scale structures in the wake that are also observed in instantaneous visualisations. A phase shift in the streamwise velocity field of that mode occurs on the upper side between the wake and freestream. Modes at lower frequencies

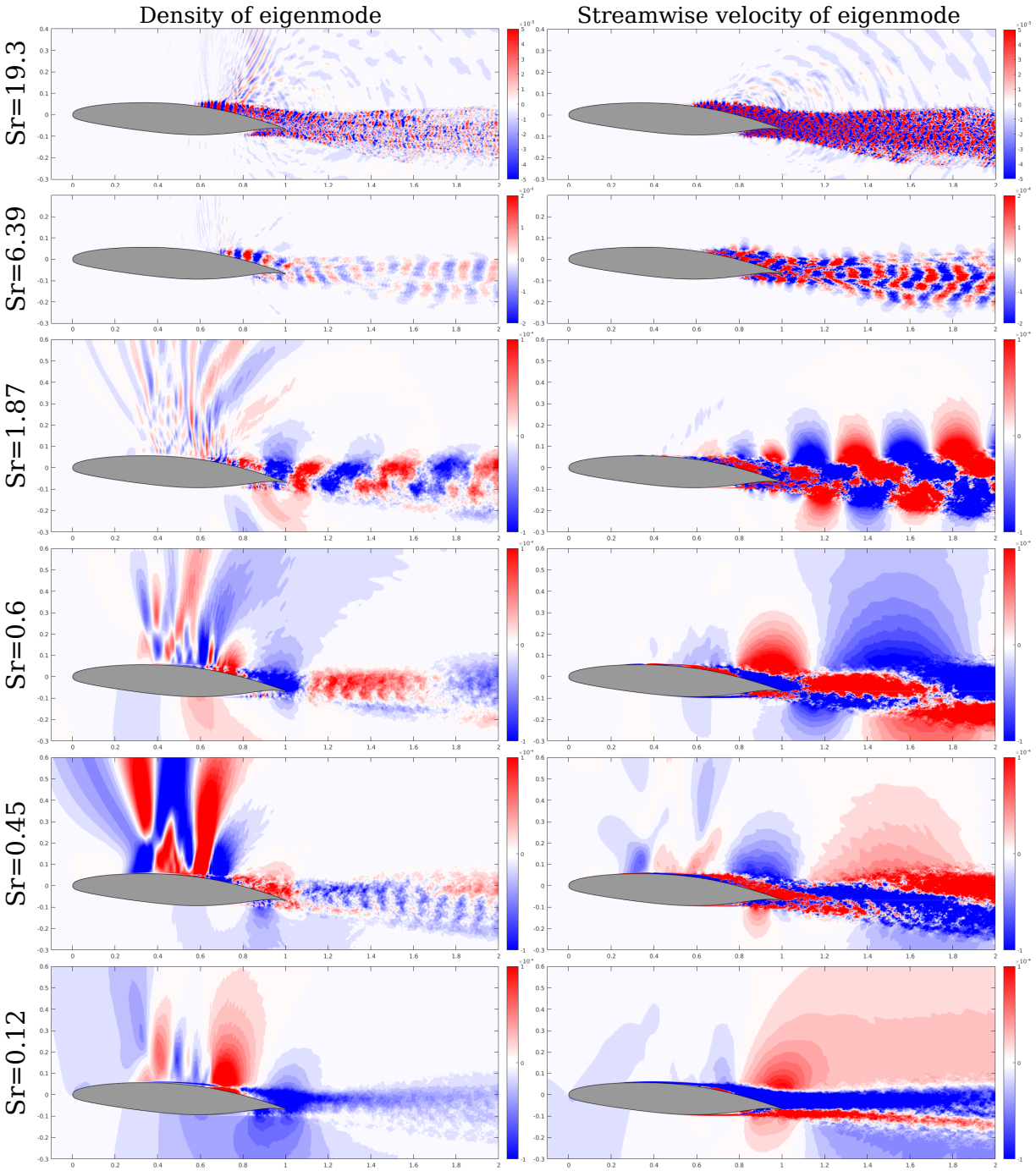

Figure 7: Selected DMD eigenmodes at different frequencies. The left and right columns show the density (ρ) and streamwise velocity (u) field, respectively.

with $St < 1$ have similar structures with high amplitudes in similar regions and correspond to flapping of the whole separated shear layers. Given the occurance of significant additional modes at roughly four and five times the buffet frequency, there is a possibility that the observed transonic buffet is a phenomenon involving multiple modes at low frequencies (including the most amplified mode at $St = 0.12$) forming a triadic interaction, rather than a phenomenon at one frequency.

Acknowledgments

We are grateful for computational resources provided by ARCHER (Leadership grant entitled Transonic flow over an aerofoil), UKTC (EPSRC grant EP/L000261/1) and Iridis (University of Southampton).

References

[1] B. H. K. Lee. Self-sustained shock oscillations on airfoils at transonic speeds. *Progress in*

Aerospace Sciences, 37:147–196, 2001.

[2] N. F. Giannelis, G. A. Vio, and O. Levinski. A review of recent developments in the understanding of transonic shock buffet. *Progress in Aerospace Sciences*, 92(May):39–84, jul 2017, doi:10.1016/j.paerosci.2017.05.004.

[3] M. Zauner, N. De Tullio, and N. D. Sandham. Direct numerical simulations of transonic flow around an airfoil at moderate Reynolds numbers. *Submitted to the AIAA Journal*, 2018.

[4] R. Placek, M. Miller, and P. Ruchała. The Roughness Position Influence on Laminar Aerofoil Aerodynamic Characteristic in Transonic Flow Regime. In *Proceedings of the 30th Congress of the International Council of the Aeronautical Sciences*, number Figure 1, pages 2–6, 2016.

[5] D. Szubert, I. Asproulias, F. Grossi, R. Duvigneau, Y. Hoarau, and M. Braza. Numerical study of the turbulent transonic interaction and transition location effect involving optimisation around a supercritical aerofoil. *European Journal of Mechanics - B/Fluids*, 55:380–393, jan 2016, doi:10.1016/j.euromechflu.2015.09.007.

[6] J. Sznajder and T. Kwiatkowski. Analysis of effects of shape and location of micro-turbulators on unsteady shockwave-boundary layer interactions in transonic flow. *Journal of KONES Powertrain and Transport*, 23(2):373–380, jan 2016, doi:10.5604/12314005.1213755.

[7] J. D. Crouch, A. Garbaruk, and D. Magidov. Predicting the onset of flow unsteadiness based on global instability. *Journal of Computational Physics*, 224(2):924–940, 2007, doi:10.1016/j.jcp.2006.10.035.

[8] S. Deck. Numerical simulation of transonic buffet over an airfoil. *AIAA journal*, 43(7):1556–1566, 2005, doi:10.2514/1.9885.

[9] E. Garnier and S. Deck. Large-eddy simulation of transonic buffet over a supercritical airfoil. In *Notes on Numerical Fluid Mechanics and Multidisciplinary Design*, volume 110, pages 135–141, 2010.

[10] S. Timme and R. Thormann. Towards Three-Dimensional Global Stability Analysis of Transonic Shock Buffet. *AIAA Atmospheric Flight Mechanics Conference*, (June):1–13, 2016, doi:10.2514/6.2016-3848.

[11] A. Sansica. Stability and Unsteadiness of Transitional Shock-Wave/Boundary-Layer Interactions in Supersonic Flows. *PhD Thesis, University of Southampton*, pages 179–184, 2015.

[12] N. De Tullio and N. D. Sandham. Global stability and transition to turbulence of separation bubbles over swept wings. *submitted to Journal of Fluid Mechanics*, 2018.

[13] M. Zauner and N. D. Sandham. PolyGridWizZ Beta-version 0.0.1. 2018, doi:10.5281/ZENODO.1245598.

[14] M. Zauner, C. T. Jacobs, and N. D. Sandham. Grid refinement using spectral error indicators with application to airfoil DNS. In *ECCM-ECFD Conference proceedings*, Glasgow, 2018.

[15] M. Zauner, N. D. Sandham, A. P. S. Wheeler, and R. D. Sandberg. Linear Stability Prediction of Vortex Structures on High Pressure Turbine Blades. *International Journal of Propulsion and Power*, 2(8), 2017, doi:10.3390/ijtpp2020008.

[16] V. Hernandez, J. E. Roman, and V. Vidal. SLEPc: A Scalable and Flexible Toolkit for the Solution of Eigenvalue Problems. *ACM Transactions on Mathematical Software*, 31(3):351–362, 2005, doi:10.1145/1089014.1089019.

[17] M. S. Hemati, M. O. Williams, and C. W. Rowley. Dynamic mode decomposition for large and streaming datasets. *Physics of Fluids*, 26(11):1–7, 2014, doi:10.1063/1.4901016.

[18] P. J. Schmid. Dynamic mode decomposition of numerical and experimental data. *Journal of Fluid Mechanics*, 656(July 2010):5–28, 2010, doi:10.1017/S0022112010001217.

[19] M. Zauner, N. De Tullio, and N. D. Sandham. Unsteady behaviour in direct numerical solutions of transonic flow around an airfoil. In *2018 AIAA Aviation Forum*, pages 1–14, 2018.

[20] L. Jones, R. Sandberg, and N. Sandham. Direct numerical simulations of forced and unforced separation bubbles on an airfoil at incidence. *Journal of Fluid Mechanics*, 602:175–207, 2008, doi:10.1017/S0022112008000864.

[21] M. Fosas De Pando, P. J. Schmid, and D. Sipp. On the receptivity of aerofoil tonal noise: An adjoint analysis. *Journal of Fluid Mechanics*, 812:771–791, 2017, doi:10.1017/jfm.2016.736.

[22] M. Fosas De Pando, P. J. Schmid, and D. Sipp. A global analysis of tonal noise in flows around aerofoils. *Journal of Fluid Mechanics*, 754:5–38, 2014, doi:10.1017/jfm.2014.356.